Efficient High Cone-Angle Artifact Reduction in Circular Cone-Beam CT using Deep Learning with Geometry-Aware Dimension Reduction

Jordi Minnema[a], Maureen van Eijnatten[b,c], Henri der Sarkissian[c], Shannon Doyle[c], Juha Koivisto[d], Jan Wolff[e,f,g], Tymour Forouzanfar[a], Felix Lucka[c,h], Kees Joost Batenburg[c,i]

[a]Amsterdam UMC and Academic Centre for Dentistry Amsterdam (ACTA), Vrije Universiteit Amsterdam, Department of Oral and Maxillofacial Surgery/Pathology, 3D Innovationlab, Amsterdam Movement Sciences, 1081 HV Amsterdam, The Netherlands
[b]Medical Image Analysis Group, Department of Biomedical Engineering, Eindhoven University of Technology, P.O. Box 513, 5600 MB Eindhoven, The Netherlands
[c]Centrum Wiskunde & Informatica (CWI), 1090 GB Amsterdam, The Netherlands
[d]Department of Physics, University of Helsinki, Gustaf Hällsströmin katu 2, FI-00560, Helsinki, Finland
[e]Department of Oral and Maxillofacial Surgery, Division for Regenerative Orofacial Medicine, University Hospital Hamburg-Eppendorf, 20246 Hamburg, Germany
[f]Fraunhofer Research Institution for Additive Manufacturing Technologies IAPT, Am Schleusengraben 13,21029 Hamburg, Germany
[g]Department of Dentistry and Oral Health, Aarhus University, Vennelyst Boulevard 9, DK-8000 Aarhus C, Denmark
[h]Centre for Medical Image Computing, University College London, WC1E 6BT London, United Kingdom
[i]Leiden Institute of Advanced Computer Science (LIACS), Leiden University, 2333 CA Leiden, The Netherlands

Corresponding author:
Jordi Minnema, MSc
Amsterdam UMC, Location VUmc
De Boelelaan 1117,
1081 HV Amsterdam, Netherlands
Tel: +31 681073639
Mail: jordi.minnema@live.nl

Abstract

High cone-angle artifacts (HCAAs) appear frequently in circular cone-beam computed tomography (CBCT) images and can heavily affect diagnosis and treatment planning. To reduce HCAAs in CBCT scans, we propose a novel deep learning approach that reduces the three-dimensional (3D) nature of HCAAs to two-dimensional (2D) problems in an efficient way. Specifically, we exploit the relationship between HCAAs and the rotational scanning geometry by training a convolutional neural network (CNN) using image slices that were radially sampled from CBCT scans. We evaluated this novel approach using a dataset of input CBCT scans affected by HCAAs and high-quality artifact-free target CBCT scans. Two different CNN architectures were employed, namely U-Net and a mixed-scale dense CNN (MS-D Net). The artifact reduction performance of the proposed approach was compared to that of a Cartesian slice-based artifact reduction deep learning approach in which a CNN was trained to remove the HCAAs from Cartesian slices. In addition, all processed CBCT scans were segmented to investigate the impact of HCAAs reduction on the quality of CBCT image segmentation. We demonstrate that the proposed deep learning approach with geometry-aware dimension reduction greatly reduces HCAAs in CBCT scans and outperforms the Cartesian slice-based deep learning approach. Moreover, the proposed artifact reduction approach markedly improves the accuracy of the subsequent segmentation task compared to the Cartesian slice-based workflow.

Keywords: artifact reduction; cone-beam computed tomography; deep learning; convolutional neural networks

Introduction

Circular cone-beam computed tomography (CBCT) is becoming an increasingly popular imaging modality in dentistry and maxillofacial surgery due to its short scanning times, low costs and low radiation doses compared to conventional computed tomography (CT) scanners (Venkatesh and Venkatesh Elluru 2017). A well-known problem in circular CBCT imaging is the high cone-angle artifact (HCAA), also referred to as the cone-beam artifact. These artifacts occur because projection data acquired in a circular X-ray source trajectory are not complete: the Tuy-Smith data sufficiency condition is not satisfied (Tuy 1983, Smith 1985). This implies that it is impossible to exactly reconstruct data points outside the midplane, i.e., the plane in which X-ray source and projector rotate. Therefore, approximate methods such as the Feldkamp-David-Kress (FDK) (Feldkamp *et al* 1984) algorithm are commonly used. However, these approximations typically lead to streaking artifacts and image distortions that become more severe with increasing cone angles (Scarfe and Farman 2008). Figure 1 presents a schematic overview of the circular CBCT image acquisition and reconstruction process of a walnut using the FDK algorithm.

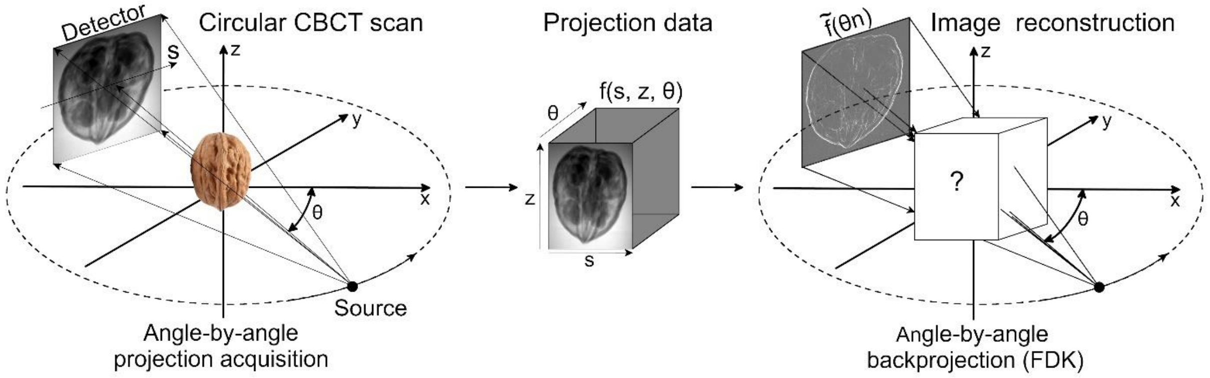

Figure 1: Schematic illustration of the CBCT image acquisition and reconstruction process with a circular X-ray source trajectory. The source and detector rotate around the object (e.g., a patient or in this case a walnut), and 2D X-ray projections of the object are acquired angle by angle. The 3D projection data volume *f* is indexed by the vertical and horizontal detector coordinates z and s, and angle θ. The order of operations in the FDK algorithm mirrors that of the data acquisition: each filtered 2D X-ray projection is backprojected angle by angle and added to the reconstructed CT volume.

Over the past decades, various approaches have been proposed to reduce HCAAs. For example, Grass et al. developed a modified FDK algorithm that rearranges the pixels in cone-beam projections into fan-shaped projections (Grass *et al* 2000). Another popular approach is to reconstruct CBCT scans using iterative reconstruction (IR) methods (Karimi and Ward 2017, Sidky and Pan 2008). Although IR algorithms generally result in fewer HCAAs (Maass *et al* 2010) and higher signal-to-noise ratios (Gardner *et al* 2019) compared to FDK reconstruction, they require much longer reconstruction times, which limits their clinical feasibility (Tang *et al* 2018, Hsieh *et al* 2013). Hu et al. and Zhu et al. independently proposed cone-angle artifact reduction approaches in which missing CBCT projection data were estimated (Hu 2006, Zhu *et al* 2008). However, this approach resulted in residual artifacts due to incorrect estimation of high-frequency Radon space data (Zhu *et al* 2008). Another way to reduce HCAAs is the two-pass approach initially developed by Hsieh (Hsieh 2000), in which high-density structures in FDK-reconstructed CBCT scans are segmented using global thresholding, followed by a simulation and subtraction of the HCAAs from the CBCT scans. This two-pass approach was recently expanded to a multi-pass approach by Han and Baek (Han and Baek 2019),who performed multiple segmentations to iteratively subtract HCAAs from the CBCT scans. However, these manually designed artifact reduction techniques require expert domain knowledge on the precise structure of the information in the measured data.

In recent years, the field of image artifact reduction has transitioned from manually designed image artifact reduction techniques reflecting expert domain knowledge to training deep neural networks. In particular convolutional neural networks (CNNs) have been employed to reduce a wide variety of CBCT image artifacts, such as metal artifacts (Gjesteby *et al* 2017, Claus *et al* 2017, Minnema *et al* 2019), scatter-induced artifacts (Jiang *et al* 2019, Maier *et al* 2018, Griner *et al* 2020), and noise (Burger *et al* 2012). The main advantage of CNNs over alternative methods is that they can learn to automatically compute a generalized mapping between artifact-affected input images and artifact-free target images. However, training CNNs to process full high-resolution three-dimensional (3D) image volumes remains computationally prohibitive and requires a large amount of suitable 3D training data. As a consequence, the feasibility of such fully 3D CNNs is extremely limited in clinical settings, where predictions are needed promptly. In order to circumvent this problem, CNNs are commonly trained on Cartesian two-dimensional (2D) image slices extracted from 3D volumes.

The reduction of HCAAs in Cartesian image slices is, however, subject to difficulties not seen with other imaging artifacts. One principled problem is that the HCAAs in a particular Cartesian slice often originate from image structures in other slices. As a consequence, the contextual information needed to remove the artifacts is lacking. Another difficulty is the fact that the severity of HCAAs depends on the distance between the Cartesian slice and the midplane (Figure 2) and thus greatly differs between slices. We hypothesize that this variability impairs the CNN's ability to learn a generalized mapping between input and target CBCT slices, which subsequently results in incomplete artifact reduction or secondary artifacts. One way of reducing this variability is to train separate CNNs for each Cartesian slice position. However, this is computationally extremely challenging and requires far more training data since only a single 2D training slice would be extracted from each 3D volume. Another way of reducing the variability using expert domain knowledge was presented by Han et al. (Han *et al* 2020). who used a CNN to process slices of the differentiated backprojection domain in different Cartesian slices, after which the slices were combined by a spectral blending technique.

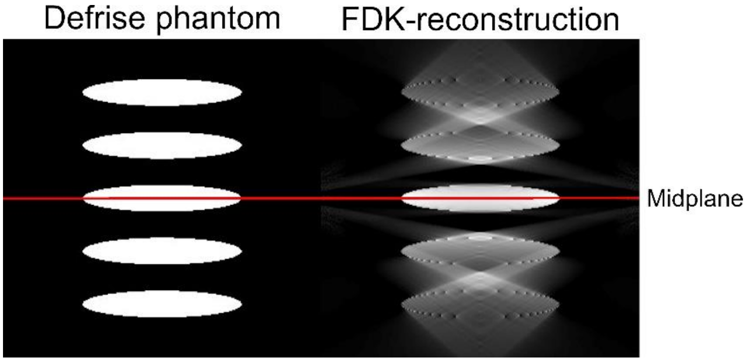

Figure 2: Illustration of the high cone-angle artifact in a Defrise phantom with five ellipses and a maximum cone-angle of 25°. Increasing the distance between the ellipse and the midplane produces stronger HCAAs in the reconstructed volume.

In this study, we propose a simpler approach to reduce high HCAAs in CBCT scans using deep learning by exploiting the most basic property of the CBCT scanning trajectory: its rotational geometry. The rotational nature of data acquisition in CBCT combined with the angle-wise backprojection performed by the FDK algorithm (Figure 1) leads to HCAAs that share the same rotational geometry. Therefore, we suggest that this rotational geometry should also be retained when post-processing the CBCT scans. To this end, we developed a workflow in which we sample 2D radial CBCT slices (i.e., angle by angle), instead of processing conventional 2D Cartesian slices to train a CNN. Radially sampled slices exhibit much less variation in HCAAs than Cartesian slices, which simplifies the cone-angle artifact reduction task. In addition, a large number of radial slices can be extracted from a single 3D volume, which further facilitates CNN training. The proposed combination of deep learning with geometry- and context-aware dimension reduction thus allows processing of high-resolution 3D CBCT volumes by 2D CNNs with high accuracy and computational efficiency.

The main contributions of this study are as follows:

- We propose a CBCT imaging pipeline consisting of the following steps: direct FDK reconstruction of radial image slices, followed by a 2D CNN and re-sampling of the radial slices into a regular 3D volume.
- This approach was evaluated using a large, publicly available, experimental CBCT dataset specifically designed to examine cone-angle artifact reduction techniques. For each CBCT scan that was reconstructed using projection data from a single X-ray source trajectory, a high-quality, HCAA-free target scan is available that was acquired by combining the single-trajectory projection data with projection data from two additional trajectories using an IR scheme.
- The results of this study show that the proposed radial slicing approach improves the artifact reduction performance of CNNs compared to traditional Cartesian slicing in terms of quantitative error measures and visual image quality. In addition, we demonstrate that this process leads to substantial improvements in image segmentation performance, which is currently the most commonly performed image processing task in clinical settings (Maier-Hein *et al* 2018).

2. Materials and Methods

Our proposed high cone-angle artifact reduction approach is based on a direct reconstruction of radial slices using the FDK algorithm. These radial slices are subsequently processed by a CNN, after which they are re-sampled into a Cartesian volume. The proposed artifact reduction workflow was compared to a Cartesian slice-based artifact reduction workflow, in which a standard FDK-reconstructed volume is sliced orthogonally (i.e., axial, sagittal or coronal) and each slice is processed by a CNN. The Cartesian slice-based workflow and the proposed artifact reduction workflow are illustrated in Figure 3.

In order to evaluate both artifact reduction workflows, a CBCT dataset was required consisting of input scans that were heavily affected by HCAAs and high-quality target scans without HCAAs. To this end, we used a publicly available CBCT data collection containing 42 scans of walnuts described in a previous publication (Der Sarkissian *et al* 2019). This data collection was specifically acquired with the purpose of benchmarking HCAA reduction algorithms. The advantage of using walnuts over anthropomorphic phantoms or manufactured objects is that they exhibit a natural variability. Moreover, since walnuts consist of a hard shell, soft core and air-filled cavities, they resemble the structure of the human skull (Hämäläinen *et al* 2015).

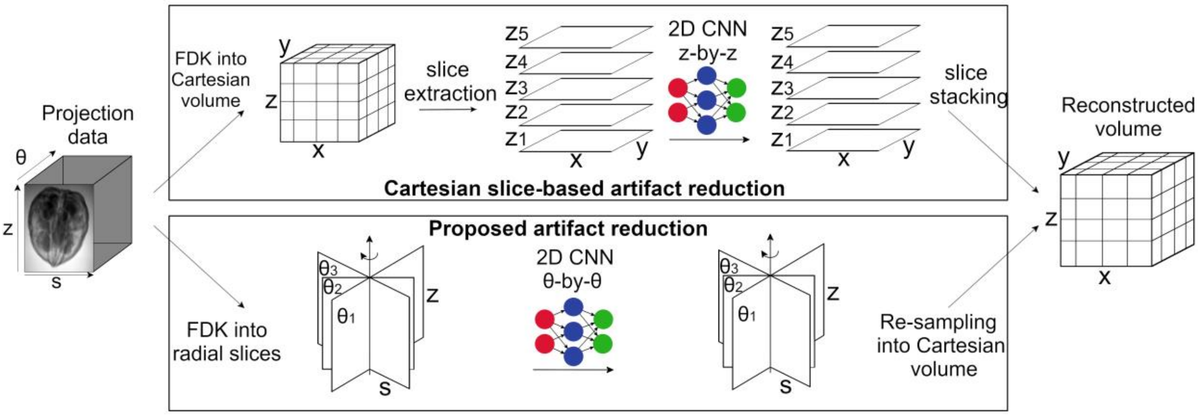

Figure 3: Schematic overview of a Cartesian slice-based workflow and the proposed cone-angle artifact reduction workflow.

2.1 Data acquisition

The input CBCT scans were obtained by scanning all 42 walnuts using a custom-built cone-beam CT scanner (FleX-ray) (Coban *et al* 2020), with a tube voltage of 40 kV and a tube current of 0.3 mA. To ensure that that the CBCT scans were affected by severe HCAAs, the vertical cone-angle was maximized by moving the samples as close as possible to the X-ray source. This resulted in a maximum cone-angle of 20°, which is comparable to cone-angles found in clinical CBCT scanners (Sheth *et al* 2020, Li *et al* 2018). In addition, the X-ray source height was chosen such that the midplane was close to the bottom part of the walnuts, which induced severe artifacts in the upper parts of the scans (Figure 4). A total of 1201 cone-beam projections were acquired and used to reconstruct CBCT scans with a volume size of 501x501x501 and an isotropic voxel size of 0.1 mm using the FDK algorithm implemented in the ASTRA Toolbox (van Aarle *et al* 2016). These reconstructed CBCT scans served as input data to train the CNN in this study.

In order to acquire high-quality target CBCT scans, all 42 walnuts were also scanned at 15 mm and 30 mm above the initial source height. The projection data obtained from the three different source positions were used to iteratively reconstruct CBCT scans by solving a non-negativity constrained least-squares problem with 50 iterations of Nesterov accelerated gradient descent (Der Sarkissian *et al* 2019, Chambolle and Pock 2016). Since three different X-ray source trajectories were used, projections with relatively small cone-angles were available for all parts of the walnut. By combining these projections, high-quality artifact-free target CBCT scans were acquired that offered high contrast and signal-to-noise ratios. Examples of the input and target CBCT scan used in this study are presented in Figure 4.

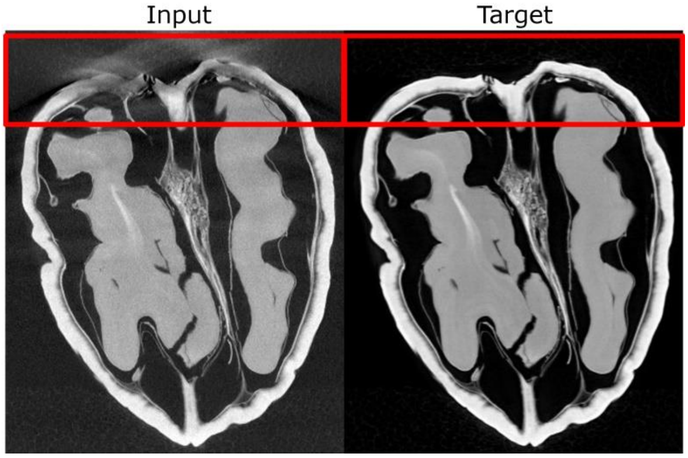

Figure 4: Examples of an input and target CBCT scan used to train the CNNs in this study. The red boxes indicate the regions of interest that were particularly affected by high HCAAs.

In order to obtain the data for the proposed cone-angle artifact reduction workflow, radial CBCT slices needed to be reconstructed from the projection data. Although it is relatively straight-forward to implement an FDK algorithm that directly reconstructs radial slices (Vanrompay *et al* 2020, Buurlage *et al* 2018), we aimed to first prove the concept of the proposed workflow. For this purpose, we interpolated radial slices from the Cartesian input and target volumes described above. To minimize interpolation artifacts, we only extracted slices close to the central x- and y-axes of the Cartesian volumes, i.e., for radial angles θ close to 0° and 90°. In order to acquire slices from the whole range of radial angles, we artificially rotated the scanning geometry and again extracted radial slices close to 0° and 90°. This process was repeated 24 times, such that a total of 709 radial slices were acquired per reconstructed volume. We used a larger number of radial slices compared to Cartesian slices (709 vs. 501) to ensure that the radial-to-Cartesian re-sampling (section 2.3. Experiments) performed after the cone-angle artifact reduction step (Figure 3) would not result in secondary artifacts.

2.2 CNN architectures

Two different CNN architectures were used to evaluate the proposed artifact reduction workflow. First, we employed the widely-used U-Net. Since U-Net consists of a relatively high number of trainable parameters it tends to overfit when the training set is relatively small (Pelt and Sethian 2018). Therefore, we also used a mixed-scale dense convolutional neural network (MS-D Net) developed by Pelt and Sethian (Pelt and Sethian 2018). The MS-D Net uses densely connected convolutional layers to directly pass important feature maps to deeper layers of the network. Information from various scales is aggregated by dilating convolutions instead of using explicit up- and down-sampling layers. As a result, MS-D Net has far fewer trainable parameters compared to U-Net, which reduces the risk of overfitting (Pelt and Sethian 2018).

We used publicly available U-Net and MS-D Net implementations (Hendriksen 2019, Milesial 2019) that are based on the deep learning framework PyTorch (v. 1.4.0) for Python (v. 3.7.3). The U-Net employed in the present study was modified in two ways compared to the original U-Net architecture proposed by Ronneberger et al. (Ronneberger *et al* 2015). First, reflective padding was applied on all input images of which the dimensions were not divisible by 16, since the U-Net would not be able to process these images otherwise. Second, batch normalization (Ioffe and Szegedy 2015) was performed before each ReLU activation function. The MS-D Net used in this study was the same as the one described by Pelt and Sethian (Pelt and Sethian 2018) with a width of 1. Training of the network was performed using a batch size of 4 for the U-Net, and a batch size of 1 for the MS-D network. In addition, training was performed using the default Adam (Kingma and Ba 2014) optimizer on a server with 192 GB RAM and one NVidia GeForce GTX 1080 Ti GPU. More detailed implementation details and justification of the chosen network parameters can be found in the supplementary materials.

2.3 Experiments

The Cartesian slice-based artifact reduction workflows and the proposed artifact reduction workflow (Figure 3) were evaluated in this study. For this purpose, we divided the 42 available CBCT scans into a training set comprising 28 scans, a validation set comprising 7 scans, and a test set comprising 7 scans.

The validation set was used to determine the number of epochs necessary to train the MS-D Net and the U-Net. The best model performances were achieved after 40 epochs for U-Net, and 60 epochs for MS-D Net. The validation set was also used to optimize the number of layers in the MS-D Net. Specifically, the number of layers was varied between 10 and 100 with a step size of 10. The number of layers, i.e., 80, was chosen such that the MS-D Net achieved the highest performance on the validation set. The training process of U-Net and MS-D Net took approximately 47 minutes and 107 minutes per epoch, respectively, whereas the processing of all slices in one CBCT scan using the trained networks took approximately 27 seconds and 34 seconds, respectively.

The trained CNNs were subsequently used to reduce artifacts in the seven CBCT scans of the test set. To ensure that differences in artifact reduction performance were not due to randomness in the initialization of the CNNs' trainable parameters, both the U-Net and the MS-D Net were independently initialized and trained five times. To enable fair comparison between the two artifact reduction workflows, all processed radial slices were resampled into a Cartesian volume using linear interpolation. The code used for the radial-to-Cartesian re-sampling is publicly available online (Minnema and Lucka 2020).

2.4 Performance evaluation metrics

The cone-angle artifact reduction achieved using the proposed artifact reduction workflow was compared to those of Cartesian slice-based artifact reduction workflows based on axial, sagittal and coronal slicing. As an additional benchmark, we applied the Nesterov accelerated gradient descent reconstruction algorithm to the projection data acquired using only the lowest X-ray source position (see section 2.1: Data acquisition). We will refer to this method as the iterative reconstruction (IR) approach. Furthermore, we included the FDK-reconstructed input CBCT scans in the comparison. The cone-angle artifact reduction performances were evaluated by computing the structural similarity (SSIM) index (Wang *et al* 2004) and the mean-squared error (MSE) between the artifact-free target CBCT scans and the output of each approach. These metrics have been commonly used to assess the quality of medical images including CBCT scans (Venkat Narayana Rao, T. and Govardhan 2013).

In addition to these generic image quality metrics, we examined the impact of the artifact reduction on a concrete, clinically-relevant image processing task. Since CBCT scans are being increasingly used for human skull segmentation (Minnema *et al* 2019) and the walnuts used in this study were chosen as proxies for the human skull, we assessed the impact of the proposed approach on the accuracy of CBCT image segmentation. For this purpose, Otsu's thresholding method (Otsu 1979) was used to segment all CBCT scans into 3 different classes: background, soft inner walnut structures and the hard outer shell. Evaluation of this segmentation step was performed by calculating the Dice Similarity Coefficient (DSC) between the segmented target CBCT scans and the CBCT scans segmented after cone-beam artifact reduction. Since the HCAAs were most severe in the upper parts of the CBCT scans, all three metrics (i.e., SSIM, MSE and DSC) were also computed for this specific region of interest (ROI), which is indicated by the red boxes in Figure 4. All metrics were calculated for the seven CBCT scans in the test set. The metrics obtained using the trained CNN's (i.e., U-Net and MS-D Net) were averaged over the five independent runs.

Results

The SSIMs, MSEs and DSCs obtained using the different cone-angle artifact reduction approaches are summarized in Table 1 and Table 2. Of all evaluated approaches, the proposed geometry-aware artifact reduction workflow generally resulted in the highest mean SSIMs and mean DSCs, and the lowest mean MSEs. The FDK-reconstructed input CBCT scans always resulted in the lowest SSIMs and DSCs, and the highest MSEs. When analyzing the full CBCT scans (i.e., no ROI), the IR approach resulted in SSIMs that were comparable or higher than all other evaluated approaches, whereas the IR approach was outperformed by all deep learning approaches when analyzing the ROI in the upper part of the scans. The proposed artifact reduction workflow generally resulted in higher mean SSIMs and lower mean MSEs compared to the Cartesian slice-based workflows. However, the proposed artifact reduction workflow resulted in lower mean DSCs than the horizontal slice-based workflow.

Figure 5 shows examples of HCAA reduction in CBCT slices, and the corresponding segmentations. All CBCT scans processed with the deep learning approaches demonstrated reduced HCAAs. More specifically, the proposed artifact reduction workflow produced CBCT scans that closely resembled the target CBCT scans and generally resulted in less residual HCAAs when compared to those produced by the Cartesian slice-based artifact reduction approach. The Cartesian slice-based approaches produced secondary artifacts (Figure 6) in the majority of CBCT scans, which significantly affected their image qualities. The IR approach generally produced high-quality CBCT scans with low noise levels, but failed to remove the HCAAs from the upper parts of the scans. Figure 7 shows an example of a radial slice and an axial slice obtained through the radial-to-Cartesian interpolation step in the proposed HCAA reduction workflow. The interpolation step did not result in any notable artifacts.

Table 1: Structural similarity (SSIM) index (± standard deviation) and the mean-squared error (MSE) (± standard deviation) produced by the different artifact reduction approaches.

	SSIM		MSE (x10^{-6})	
	Full volumes	ROI	Full volumes	ROI
Input - FDK	0.679 ± 0.067	0.547 ± 0.079	15.12 ± 2.58	55.50 ± 8.15
IR approach	**0.963 ± 0.009**	0.870 ± 0.030	5.04 ± 1.25	27.54 ± 6.54
U-Net				
Axial	0.919 ± 0.028	0.918 ± 0.040	19.70 ± 15.21	8.56 ± 3.12
Sagittal	0.930 ± 0.039	0.945 ± 0.029	41.11 ± 43.10	13.43 ± 10.32
Coronal	0.956 ± 0.020	0.943 ± 0.031	2.61 ± 0.97	6.51 ± 2.14
Proposed	0.957 ± 0.047	**0.953 ± 0.017**	2.59 ± 0.76	6.38 ± 3.12
MS-D Net				
Axial	0.947 ± 0.029	0.920 ± 0.032	2.88 ± 1.43	8.50 ± 3.33
Sagittal	0.953 ± 0.017	0.915 ± 0.035	3.04 ± 1.26	7.93 ± 2.77
Coronal	0.942 ± 0.023	0.904 ± 0.049	3.96 ± 2.50	10.1 ± 3.65
Proposed	0.949 ± 0.021	0.932 ± 0.031	**2.56 ± 0.70**	**5.71 ± 2.37**

Table 2: Mean Dice similarity coefficients (DSC) (± standard deviation) of the segmented low-density inner structures and high-density outer structures.

	DSC – low density structures		DSC – high density structures	
	Full volumes	ROI	Full volumes	ROI
Input - FDK	0.904 ± 0.017	0.720 ± 0.033	0.895 ± 0.022	0.682 ± 0.027
IR approach	0.911 ± 0.015	0.772 ± 0.166	0.917 ± 0.019	0.794 ± 0.025
U-Net				
Axial	0.898 ± 0.040	0.863 ± 0.130	0.913 ± 0.034	0.936 ± 0.016
Sagittal	0.914 ± 0.039	0.897 ±0.027	0.931 ± 0.044	0.918 ± 0.087
Coronal	**0.946 ± 0.016**	**0.908 ± 0.015**	**0.956 ± 0.020**	0.946 ± 0.014
Proposed	0.933 ± 0.012	0.898 ± 0.013	0.951 ± 0.013	0.945 ± 0.017
MS-D Net				
Axial	0.941 ± 0.018	0.891 ± 0.017	0.942 ± 0.061	0.933 ± 0.018
Sagittal	0.940 ± 0.019	0.896 ± 0.014	0.950 ± 0.018	0.937 ± 0.017
Coronal	0.936 ± 0.020	0.894 ± 0.032	0.945 ± 0.018	0.925 ± 0.020
Proposed	0.933 ± 0.013	0.902 ± 0.013	0.952 ± 0.013	**0.950 ± 0.014**

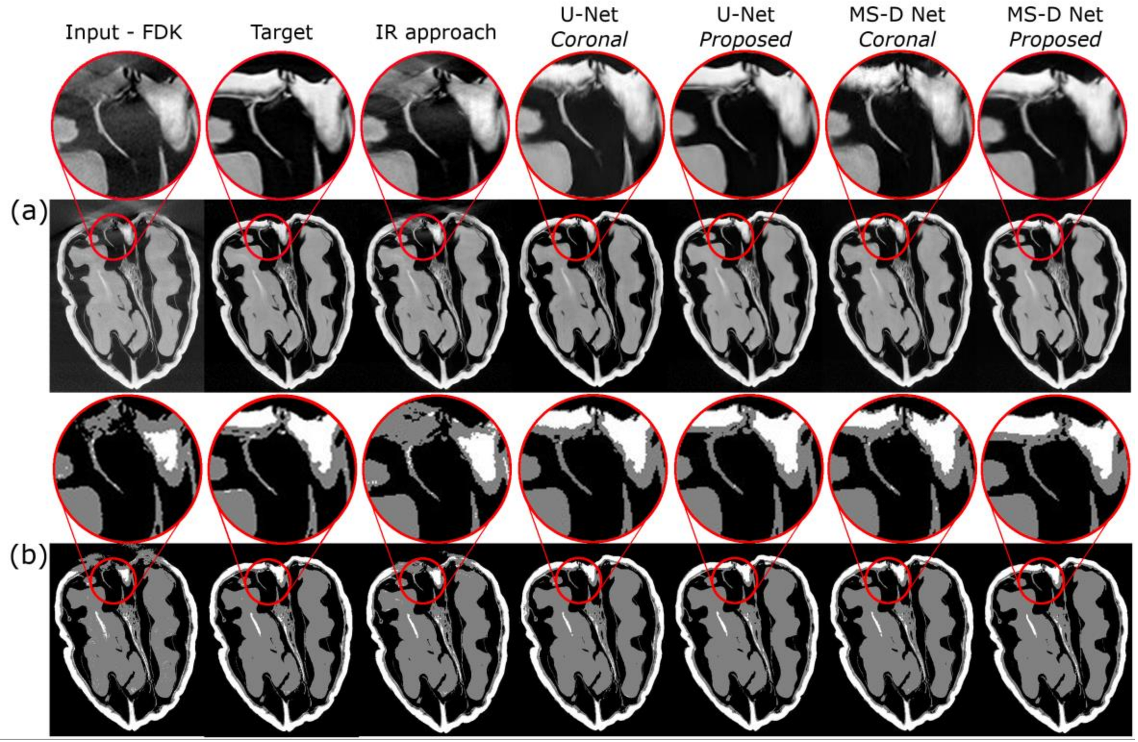

Figure 5: Example of a vertical slice of a CBCT scan processed by the HCAA reduction methods. The upper row (a) shows the output of the different artifact reduction approaches, and the bottom row (b) shows the corresponding segmented slices. Of the three evaluated Cartesian slice approaches, only the results of the coronal slice-based approach are visualized since it performed best in terms of SSIMs, MSEs and DSCs.

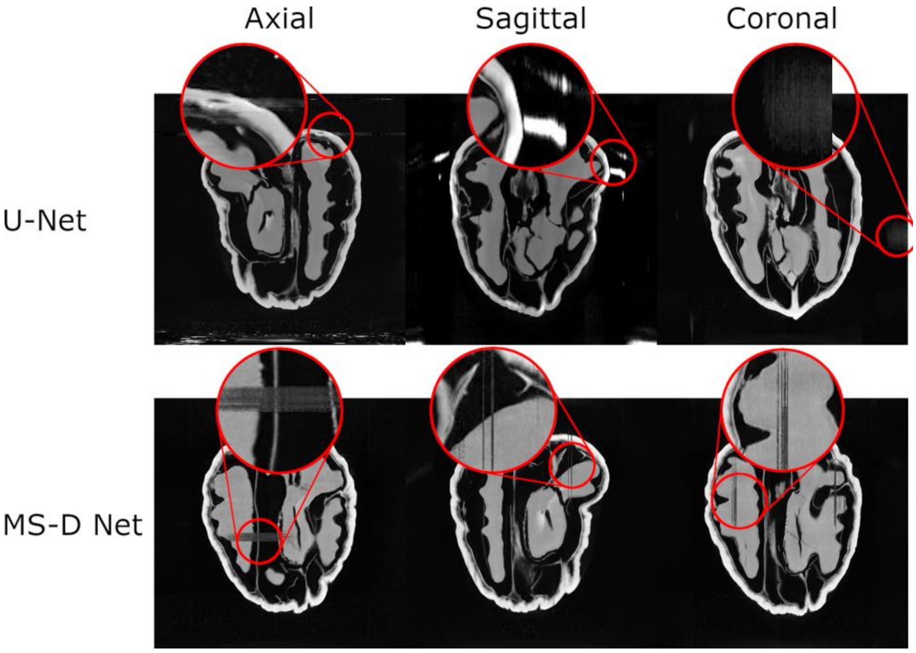

Figure 6: Examples of secondary artifacts in walnut CBCT slices produced by Cartesian slice-based workflows (i.e., axial, sagittal and coronal).

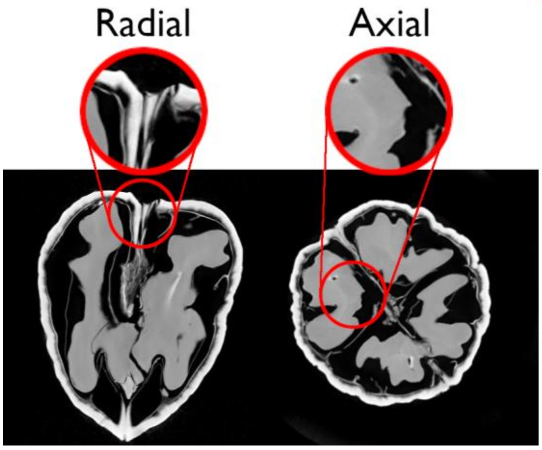

Figure 7: Example of a radial slice and an axial slice obtained through the radial-to-Cartesian interpolation step in the proposed HCAA reduction workflow.

Discussion

High HCAAs are an inherent problem of circular CBCT technology. Although deep learning has recently been successfully employed to reduce various imaging artifacts, cone-angle artifact reduction remains especially challenging. Therefore, the aim of this study was to develop a novel deep learning-based artifact reduction workflow that exploits the symmetry of HCAAs.

The proposed geometry- and context-aware artifact reduction workflow was able to reduce HCAAs in CBCT scans more effectively than the Cartesian slice-based artifact reduction workflow (Figure 5 and Figure 6). Moreover, the CNNs trained in the proposed workflow always resulted in SSIMs, MSEs and DSCs that were comparable or better than those obtained using the IR approach (Table 1 and Table 2). The primary reason why the proposed workflow resulted in better HCAA reduction is that radial slicing provides a more efficient dimension reduction from 3D to 2D compared to Cartesian slicing: the HCAAs exhibit much less spatial variation in radial slices compared to Cartesian slices, and radial slices offer more relevant context to remove the HCAAs. This facilitates the training process of a CNN and enables the learning of a generalized mapping between artifact-affected input scans and artifact-free target scans.

An interesting finding in this study was that the Cartesian slice-based artifact reduction workflows resulted in unexpectedly severe secondary artifacts in the majority of the CBCT scans (Figure 6). This phenomenon was observed when using both U-Net and MS-D Net. Since the secondary artifacts manifested as clearly distinguishable streaks in the Cartesian planes, it is likely that the CNNs failed to correctly process the corresponding Cartesian slices of those CBCT scans. A possible explanation for this finding is that the CNNs tried to reduce HCAAs in all slices of the CBCT scan, even if those slices were not affected by HCAAs. After all, since the CNNs had no contextual information on the position of the 2D slices within the CBCT scan, it might have been difficult to distinguish artifact-affected slices from artifact-free slices.

A major advantage of using CNNs for cone-angle artifact reduction is the low computational time required to process CBCT scans compared to more traditional methods such as the IR approach. More specifically, the time needed to process one CBCT scan in this study was approximately 27 seconds for U-Net and 34 seconds for MS-D Net, whereas the IR approach took approximately 20 minutes to reconstruct a CBCT scan (512x512x512). The shorter computational times make it much easier to incorporate these CNNs approaches in clinical workflows.

Another advantage of the proposed HCAA artifact reduction workflow is its broad applicability. Since our workflow exploits basic geometrical properties of circular CBCT scanners, it is expected that this workflow is capable of accurately reducing HCAAs in CBCT scans obtained using any kind of circular CBCT scanner. Moreover, the proposed deep learning workflow may provide promising avenues to reduce HCAAs in limited-angle CBCT systems. Nevertheless, further research is necessary to determine whether CNNs trained on scans from a specific CBCT scanner can generalize to scans acquired using different CBCT scanners.

A technical challenge of employing our novel deep learning approach was the radial-to-Cartesian re-sampling step that is necessary after processing the radial CBCT slices. Although Figure 7 shows that no notable interpolation artifacts were introduced in this study, the re-sampling step remains a 2D task that is performed for each z-slice independently, which could possibly introduce minor interpolation artifacts in the CBCT scans (Aganj *et al* 2013). One way of avoiding such interpolation artifacts could be to use a deep learning-based interpolation method (Zhou *et al* 2017). Because such methods are able to memorize local structures in CBCT scans, they can recognize geometric variations and thus produce more accurate pixel estimations.

The next step towards employing the proposed artifact reduction workflow is to translate the learning procedure and the necessary data acquisition to clinical practice. A possible way of achieving this would be to perform a phantom or cadaver study and acquire high-quality target CBCT scans following the methodology of the present study, i.e., by combining projection data from three different circular X-ray trajectories. Another option would be to use helical CT scans as the high-quality target, since those are not affected by HCAAs. However, since patients are not commonly scanned using both CBCT and helical CT, it might be necessary to apply semi-supervised learning approaches such as generative adversarial networks (Maspero *et al* 2020). Another way of facilitating the application of the proposed approach in clinical settings might be through transfer learning. In such a transfer learning scheme, the CNN models trained on walnut CBCT scans could be used as the initial model, instead of randomly initializing a new model. Since the models do not need to be trained from scratch, fewer clinical CBCT scans would be necessary to learn the cone-angle artifact reduction. By translating the proposed deep learning-based cone-angle artifact reduction approach into the clinic, medical practitioners will be able to establish accurate diagnoses and create feasible treatment plans based on circular CBCT images of the patient. In addition, the proposed workflow might allow clinicians to scan larger volumes by increasing the cone-angles, which would markedly improve the applicability of circular CBCT technology.

Conclusion

This study presents a novel pipeline to reduce HCAAs in CBCT scans with deep learning. By designing a tailored dimension reduction scheme that reflects the rotational symmetry of CBCT scans, we were able to efficiently reduce 3D cone-angle artifacts in CBCT scans with 2D CNNs. The proposed HCAA reduction workflow showed to be more robust than the Cartesian slice-based workflows, while it consistently outperformed the iterative reconstruction approach. In addition, we showed that the cone-angle artifact reduction leads to considerable improvements when segmenting the CBCT scans. The results of this study will hopefully motivate clinicians and medical engineers to adopt the proposed artifact-reduction workflow in clinical settings, thereby opening up promising new avenues for a large-scale use of CBCT imaging in a wide variety of medical disciplines.

Acknowledgements

This work was supported by the Netherlands Organisation for Scientific Research (NWO) project number 639.073.506; and by Planmeca Oy. In addition, MvE, FL and KJB acknowledge financial support by Holland High Tech through the PPP allowance for research and development in the HTSM topsector.

Software availability

To increase the reproducibility of this study, we provide the Python scripts that were used for training data preparation, model training and model evaluation. These scripts will be made publicly available on Github (https://github.com/Jomigi/Cone_angle_artifact_reduction). Running the scripts requires the open-source software packages ASTRA toolbox and Pytorch, and a Graphics Processing Unit (GPU).

Conflicts of interest

The authors have no conflicts of interest to disclose.

References

van Aarle W, Palenstijn W J, Cant J, Janssens E, Bleichrodt F, Dabravolski A, De Beenhouwer J, Joost Batenburg K and Sijbers J 2016 Fast and flexible X-ray tomography using the ASTRA toolbox *Opt. Express* **24** 25129

Aganj I, Yeo B T T, Sabuncu M R and Fischl B 2013 On Removing Interpolation and Resampling Artifacts in Rigid Image Registration *IEEE Trans. on Image Process.* **22** 816–27

Burger H C, Schuler C J and Harmeling S 2012 Image denoising with multi-layer perceptrons, part 1: comparison with existing algorithms and with bounds *arXiv:1211.1544 [cs]* Online: http://arxiv.org/abs/1211.1544

Buurlage J-W, Kohr H, Jan Palenstijn W and Joost Batenburg K 2018 Real-time quasi-3D tomographic reconstruction *Meas. Sci. Technol.* **29** 064005

Chambolle A and Pock T 2016 An introduction to continuous optimization for imaging *Acta Numerica* **25** 161–319

Claus B E H, Jin Y, Gjesteby L, Wang G and De Man B 2017 Metal-Artifact Reduction Using Deep-Learning Based Sinogram Completion: Initial Results *Fully3D 2017 Proceedings* 631–5

Coban S B, Lucka F, Palenstijn W J, Van Loo D and Batenburg K J 2020 Explorative Imaging and Its Implementation at the FleX-ray Laboratory *J. Imaging* **6** 18

Der Sarkissian H, Lucka F, van Eijnatten M, Colacicco G, Coban S B and Batenburg K J 2019 A cone-beam X-ray computed tomography data collection designed for machine learning *Sci Data* **6** 215

Feldkamp L A, Davis L C and Kress J W 1984 Practical cone-beam algorithm *J. Opt. Soc. Am. A* **1** 612

Gardner S J, Mao W, Liu C, Aref I, Elshaikh M, Lee J K, Pradhan D, Movsas B, Chetty I J and Siddiqui F 2019 Improvements in CBCT Image Quality Using a Novel Iterative Reconstruction Algorithm: A Clinical Evaluation *Advances in Radiation Oncology* **4** 390–400

Gjesteby L, Yang Q, Xi Y, Claus B E H, Jin Y, De Man B, Wang G and Shan H 2017 Deep learning methods for CT image-domain metal artifact reduction *Developments in X-Ray Tomography XI* Developments in X-Ray Tomography XI ed B Müller and G Wang (San Diego, United States: SPIE) p 31

Grass M, Köhler T and Proksa R 2000 3D cone-beam CT reconstruction for circular trajectories *Phys. Med. Biol.* **45** 329–47

Griner D, Garrett J W, Li Y, Li K and Chen G-H 2020 Correction for cone beam CT image artifacts via a deep learning method *Medical Imaging 2020: Physics of Medical Imaging* Physics of Medical Imaging ed H Bosmans and G-H Chen (Houston, United States: SPIE) p 162

Hämäläinen K, Harhanen L, Kallonen A, Kujanpää A, Niemi E and Siltanen S 2015 Tomographic X-ray data of a walnut *arXiv:1502.04064 [physics]* Online: http://arxiv.org/abs/1502.04064

Han C and Baek J 2019 Multi-pass approach to reduce cone-beam artifacts in a circular orbit cone-beam CT system *Opt. Express* **27** 10108

Han Y, Kim J and Ye J C 2020 Differentiated Backprojection Domain Deep Learning for Conebeam Artifact Removal *IEEE Trans. Med. Imaging* 1–1

Hendriksen A 2019 *ahendriksen/msd_pytorch: v0.7.2* (Zenodo) Online: https://zenodo.org/record/3560114

Hsieh J 2000 Two-pass algorithm for cone-beam reconstruction Medical Imaging 2000 ed K M Hanson (San Diego, CA) pp 533–40

Hsieh J, Nett B, Yu Z, Sauer K, Thibault J-B and Bouman C A 2013 Recent Advances in CT Image Reconstruction *Current Radiology Reports* **1** 39–51

Hu H 2006 An improved cone-beam reconstruction algorithm for the circular orbit *Scanning* **18** 572–81

Ioffe S and Szegedy C 2015 Batch Normalization: Accelerating Deep Network Training by Reducing Internal Covariate Shift *arXiv:1502.03167 [cs]* Online: http://arxiv.org/abs/1502.03167

Jiang Y, Yang C, Yang P, Hu X, Luo C, Xue Y, Xu L, Hu X, Zhang L, Wang J, Sheng K and Niu T 2019 Scatter correction of cone-beam CT using a deep residual convolution neural network (DRCNN) *Phys. Med. Biol.* **64** 145003

Karimi D and Ward R K 2017 Image reconstruction in computed tomography using variance-reduced stochastic gradient descent *2017 IEEE 14th International Symposium on Biomedical Imaging (ISBI 2017)* 2017 IEEE 14th International Symposium on Biomedical Imaging (ISBI 2017) (Melbourne, Australia: IEEE) pp 543–7 Online: http://ieeexplore.ieee.org/document/7950579/

Kingma D P and Ba J 2014 Adam: A Method for Stochastic Optimization *arXiv:1412.6980 [cs]* Online: http://arxiv.org/abs/1412.6980

Li Y, Garrett J W, Li K, Wu Y, Johnson K, Schafer S, Strother C and Chen G-H 2018 Time-resolved C-arm cone beam CT angiography (TR-CBCTA) imaging from a single short-scan C-arm cone beam CT acquisition with intra-arterial contrast injection *Phys. Med. Biol.* **63** 075001

Maass C, Dennerlein F, Noo F and Kachelriess M 2010 Comparing short scan CT reconstruction algorithms regarding cone-beam artifact performance *IEEE Nuclear Science Symposuim & Medical Imaging Conference* 2010 IEEE Nuclear Science Symposium and Medical Imaging Conference (2010 NSS/MIC) (Knoxville, TN: IEEE) pp 2188–93 Online: http://ieeexplore.ieee.org/document/5874170/

Maier J, Sawall S, Knaup M and Kachelrieß M 2018 Deep Scatter Estimation (DSE): Accurate Real-Time Scatter Estimation for X-Ray CT Using a Deep Convolutional Neural Network *J Nondestruct Eval* **37** 57

Maier-Hein L, Eisenmann M, Reinke A, Onogur S, Stankovic M, Scholz P, Arbel T, Bogunovic H, Bradley A P, Carass A, Feldmann C, Frangi A F, Full P M, van Ginneken B, Hanbury A, Honauer K, Kozubek M, Landman B A, März K, Maier O, Maier-Hein K, Menze B H, Müller H, Neher P F, Niessen W, Rajpoot N, Sharp G C, Sirinukunwattana K, Speidel S, Stock C, Stoyanov D, Taha A A, van der Sommen F, Wang C-W, Weber M-A, Zheng G, Jannin P and Kopp-Schneider A 2018 Why rankings of biomedical image analysis competitions should be interpreted with care *Nat Commun* **9** 5217

Maspero M, Houweling A C, Savenije M H F, van Heijst T C F, Verhoeff J J C, Kotte A N T J and van den Berg C A T 2020 A single neural network for cone-beam computed tomography-based radiotherapy of head-and-neck, lung and breast cancer *Physics and Imaging in Radiation Oncology* **14** 24–31

Milesial 2019 *Pytorch-UNet* Online: https://github.com/milesial/Pytorch-UNet

Minnema J, Eijnatten M, Hendriksen A A, Liberton N P T J, Pelt D M, Batenburg K J, Forouzanfar T and Wolff J 2019 Segmentation of dental cone-beam CT scans affected by metal artifacts using a mixed-scale dense convolutional neural network *Med. Phys.* **46** 5027–35

Minnema J and Lucka F 2020 Cone_angle_artifact_reduction *Github* Online: https://github.com/Jomigi/Cone_angle_artifact_reduction

Otsu N 1979 A Threshold Selection Method from Gray-Level Histograms *IEEE Trans. Syst., Man, Cybern.* **9** 62–6

Pelt D M and Sethian J A 2018 A mixed-scale dense convolutional neural network for image analysis *Proceedings of the National Academy of Sciences* **115** 254–9

Ronneberger O, Fischer P and Brox T 2015 U-Net: Convolutional Networks for Biomedical Image Segmentation *Medical Image Computing and Computer-Assisted Intervention – MICCAI 2015* 234–241

Scarfe W C and Farman A G 2008 What is Cone-Beam CT and How Does it Work? *Dental Clinics of North America* **52** 707–30

Sheth N M, De Silva T, Uneri A, Ketcha M, Han R, Vijayan R, Osgood G M and Siewerdsen J H 2020 A mobile isocentric C-arm for intraoperative cone-beam CT: Technical assessment of dose and 3D imaging performance *Med. Phys.* **47** 958–74

Sidky E Y and Pan X 2008 Image reconstruction in circular cone-beam computed tomography by constrained, total-variation minimization *Phys. Med. Biol.* **53** 4777–807

Smith B D 1985 Image Reconstruction from Cone-Beam Projections: Necessary and Sufficient Conditions and Reconstruction Methods *IEEE Trans. Med. Imaging* **4** 14–25

Tang X, Krupinski E A, Xie H and Stillman A E 2018 On the data acquisition, image reconstruction, cone beam artifacts, and their suppression in axial MDCT and CBCT - A review *Med. Phys.* **45** e761–82

Tuy H K 1983 An Inversion Formula for Cone-Beam Reconstruction *SIAM J. Appl. Math.* **43** 546–52

Vanrompay H, Buurlage J, Pelt D M, Kumar V, Zhuo X, Liz-Marzán L M, Bals S and Batenburg K J 2020 Real-Time Reconstruction of Arbitrary Slices for Quantitative and In Situ 3D Characterization of Nanoparticles *Part. Part. Syst. Charact.* 2000073

Venkat Narayana Rao, T. T and Govardhan A 2013 Assessment of Diverse Quality Metrics for Medical Images Including Mammography *IJCA* **83** 42–7

Venkatesh E and Venkatesh Elluru S 2017 Cone Beam Computed Tomography: Basics and Applications in Dentistry *J Istanbul Univ Fac Dent* **51** Online: http://eor.istanbul.edu.tr/tr/yazi/10-17096-jiufd-00289-45003800710045003200740059006800360077005500310 0

Wang Z, Bovik A C, Sheikh H R and Simoncelli E P 2004 Image Quality Assessment: From Error Visibility to Structural Similarity *IEEE Trans. on Image Process.* **13** 600–12

Zhou W, Li X and Reynolds D S 2017 Nonlinear image interpolation via deep neural network *2017 51st Asilomar Conference on Signals, Systems, and Computers* 2017 51st Asilomar Conference on Signals, Systems, and Computers (Pacific Grove, CA: IEEE) pp 228–32 Online: https://ieeexplore.ieee.org/document/8335172/

Zhu L, Starman J and Fahrig R 2008 An Efficient Estimation Method for Reducing the Axial Intensity Drop in Circular Cone-Beam CT *International Journal of Biomedical Imaging* **2008** 1–11